Tellus (1982), *34*, 321–333

Sensitivity of the boundary layer energy fluxes to forcing parameters in a simple climate model

By M. SANKAR RAO[1] and G. DALU[2], *Laboratory for Atmospheric Sciences (GLAS), NASA/Goddard Space Flight Center, Greenbelt, Maryland 20771, U.S.A.*, and R. C. LO, *Computer Sciences Corporation, Silver Spring, Maryland 20910, U.S.A.*

(Manuscript received July 21, 1980; in final form November 23, 1981)

ABSTRACT

Winter and summer surface temperatures and time-averaged boundary layer energy fluxes are calculated by utilizing the Saltzman-Ashe parameterization for boundary layer fluxes in a two-level static model. The results are found to agree with observed patterns. Within the framework of this simple model, sensitivity analyses of the time-averaged boundary layer energy fluxes are conducted. Based on these results some of the forcing parameters (such as the subsurface temperature, cloud cover, surface albedo etc.) are arranged in a hierarchical order of importance. A generalized method of sensitivity analysis is also suggested.

1. Introduction

The non-uniform distribution of radiative heating and cooling over the earth drives the motion of the atmosphere and oceans. Most of the energy input that drives the atmosphere is absorbed by the earth's surface and returned to the atmosphere in the form of sensible heat flux and latent heat flux. The time averaged state of the atmosphere is largely controlled by the time averages of these energy fluxes (Saltzman, 1968). These fluxes depend on a variety of factors defining the state of the atmosphere, the state of the lower boundary, and the incoming solar radiation. In some time-dependent models some parameters of the lower boundary, such as surface albedo, the thermal conductivity, etc., are usually prescribed (Manabe et al., 1965), while in some time-averaged models, the atmospheric response is obtained by iteration until an equilibrium is reached (Saltzman and Vernekar, 1971).

Experimentation with such complex models requires the assessment of a hierarchical order of importance of various input parameters for the creation of boundary forcings in the form of energy fluxes, for (a) large spatial scales that govern global circulations and (b) small spatial scales that govern local circulations. These are two different kinds of problem. A small perturbation in cloud cover, for instance, can produce a corresponding perturbation in the boundary fluxes at a particular locality, but a random perturbation of the same magnitude in cloud cover over a large area may or may not produce a significant perturbation in the average boundary layer fluxes over that area. This is due to the possibility of great variation in the background in the form of conductivity, surface albedo etc. Thus for any scale considered it is useful to assess the hierarchical order of input parameters, i.e. having fixed the accuracy of one input parameter, determine the compatible accuracy of prescription or observation in other input parameters. For example there is not much use in considering the absorption spectrum of water vapour with great accuracy if the cloud cover observations involve large inaccuracies.

The aim of this study is to answer approximately but quantitatively some of the questions on the

[1] NAS/NRC Research Associate. Permanent address: Department of Aeronautics, Indian Institute of Science, Bangalore 560012, India.

[2] NAS/NRC Research Associate. Permanent address: Istituto di Fisica dell'Atmosfera, Piazza Sturzo 31, 00144 Rome, Italy.

 0040-2826/82/040321-13$02.50/0

relative importance of input parameters for forcings on large scales. This is attempted with the help of a simple model and the theory of the surface temperature of the earth developed by Saltzman and Ashe (1976a, b). This kind of information is relevant for the design of observational systems for large-scale predictions. It is also relevant for the design of numerical models, especially in deciding whether anything can be gained by further refinement of a particular aspect (such as the boundary layer physics, radiation, cumulus convection, etc.) of a model, given a particular observational system with given levels of accuracy in the measurement of various parameters.

2. The model equations

We consider a two-level model atmosphere which does not interact dynamically with the lower surface. It interacts, however, with the lower surface thermodynamically through long-wave radiation and small-scale eddy fluxes of heat. The levels $l = 2$ and $l = 4$ correspond to 500 mb and 850 mb respectively. Then the heat balance equation, averaged over a period of the order of a month, for the earth's surface, can be written as

$$\bar{H}_{\rm SW} + \bar{H}_{\rm LW} + \bar{H}_{\rm SM} + \bar{H}_{\rm SS} + \bar{H}_{\rm SD} + \bar{H}_{\rm SD} + \bar{H}_{\rm L} + \bar{H}_{\rm D} = 0, \qquad (1)$$

where

$\bar{H}_{\rm SW}$ = mean heat flux due to short-wave radiation,
$\bar{H}_{\rm LW}$ = mean heat flux due to long-wave radiation,
$\bar{H}_{\rm SM}$ = mean part of the mean sensible heat flux,
$\bar{H}_{\rm SS}$ = synoptic part of the mean sensible heat flux caused by synoptic variation of temperature,
$\bar{H}_{\rm SD}$ = diurnal part of the mean sensible heat flux caused by diurnal variation of temperature,
$\bar{H}_{\rm L}$ = mean latent heat flux,
$\bar{H}_{\rm D}$ = mean subsurface heat flux.

The formulae for these fluxes are as follows (see Appendix for list of symbols):

$$\bar{H}_{\rm SW} = (1-\bar{\chi})(1-\bar{r}_{\rm a})(1-\bar{r}_{\rm s})R(\phi); \qquad (2)$$

$$\bar{H}_{\rm LW} = \sigma\left[(1-\beta_{\rm R}\,\bar{c})\,\text{ɰ}\left(\frac{p^2}{p_{\rm s}}\right)^{4\kappa}\bar{\theta}_2^4 - \bar{\theta}_{\rm s}^4\right]; \qquad (3)$$

$$\bar{H}_{\rm SM} = -a - b(\bar{\theta}_{\rm s} - \bar{\theta}_4), \qquad (4)$$

where

$$a = \bar{\rho}c_{\rm p}\,\gamma_{\rm c}\left[\bar{K}_0 + \frac{\bar{\varepsilon}_{\rm T}}{2\bar{Z}_{\rm F}}(|\bar{\theta}_{\rm s}-\bar{\theta}_4| + (\bar{\theta}_{\rm s}-\bar{\theta}_4))\right],$$

$$b = \frac{\bar{\rho}c_{\rm p}}{\bar{Z}_{\rm F}}\left[\bar{K}_0 + \frac{\bar{\varepsilon}_{\rm T}}{2\bar{Z}_{\rm F}}(|\bar{\theta}_{\rm s}-\bar{\theta}_4| + (\bar{\theta}_{\rm s}-\bar{\theta}_4))\right];$$

$$\bar{H}_{\rm SS} = -C_{\rm S}(1-\beta_{\rm S})^2\,\frac{A_{\rm S}}{\alpha}\,|\nabla\bar{\theta}_4|^2, \qquad (5)$$

where

$$C_{\rm S} = \bar{\rho}c_{\rm p}\,\bar{\varepsilon}_{\rm T}/\bar{Z}_{\rm F}^2,$$

$$\beta_{\rm S} = \frac{\bar{\nu}}{[(\bar{\gamma}+k_2)^2 + k_2^2]^{1/2}},$$

$$\bar{\nu} = \bar{\rho}c_{\rm p}(1 + ({\rm BOR}-1)\bar{w})\bar{Z}_{\rm F}^{-1}\left[K_0 + \frac{\bar{\varepsilon}_{\rm T}}{2\bar{Z}_{\rm F}}\times(|\bar{\theta}_{\rm s}-\bar{\theta}_4| + (\bar{\theta}_{\rm s}-\bar{\theta}_4))\right],$$

$$\bar{\gamma} = \bar{\nu} + 4A^3\sigma,$$

$$k_2 = \rho_{\rm S}\,SK_{\rm D}^{1/2}\sqrt{\tfrac{1}{2}\omega_2};$$

$$\bar{H}_{\rm SD} = -C_{\rm S}\sum_{j=1}^{6}\frac{(\bar{\mu}B_j)^2}{2[(\bar{\gamma}+k_{1j})^2 + k_{1j}^2]}, \qquad (6)$$

where

$\bar{\mu} = (1-\bar{\chi})(1-\bar{r}_{\rm a})(1-\bar{r}_{\rm s})$
= mean absorption coefficient of solar radiation at the surface,

$$k_{1j} = \rho_{\rm S}\,SK_{\rm D}^{1/2}\sqrt{\tfrac{1}{2}j\omega_1};$$

$$\bar{H}_{\rm L} = [{\rm BOR}\times\bar{H}_{\rm S} + C_{\rm S}]\bar{w}, \qquad (7)$$

where

$$\bar{H}_{\rm S} = \bar{H}_{\rm SM} + \bar{H}_{\rm SS} + \bar{H}_{\rm SD};$$

$$\bar{H}_{\rm D} = \rho_{\rm S}\,SK_{\rm D}^{1/2}\left[\bar{\theta}_{\rm s} - \bar{T}_{\rm D} - A_{\rm T}\sin\frac{2\pi}{P}t\right]. \qquad (8)$$

These parameterizations, except for $\bar{H}_{\rm LW}$, are identical to Saltzman-Ashe parameterizations. For $\bar{H}_{\rm LW}$ the parameterization is similar to that utilized in some two-level GCM's (Kurihara, 1970) for clear sky conditions. In eq. (3), the correction due to cloud cover for the downward atmospheric long-wave radiation is incorporated through an empirical multiplying factor $\beta_{\rm R}$. In general, the empirical parameters ɰ and $\beta_{\rm R}$ can at best be considered only as approximate, even for time-averaged downward atmospheric long-wave radiation calculations. For instance $\beta_{\rm R}$ can be a function of the season and of the geographical coordinates (Kondratyev, 1969). This has to be taken into account in the interpretation of the results. In $\bar{H}_{SW}$ the atmospheric albedo is taken as a function of cloud cover as given by Vernekar (1975).

If we now substitute (2)–(8) into (1) and utilize linear forms for $\bar{\theta}_2^4$ and $\bar{\theta}_s^4$, we get an algebraic equation for $\bar{\theta}_s$ as follows:

$$C_1 \bar{\theta}_s + C_2 + C_{1T}(|\bar{\theta}_s - \bar{\theta}_4| + (\bar{\theta}_s - \bar{\theta}_4)) + C_{2T}(|\bar{\theta}_s - \bar{\theta}_4| + (\bar{\theta}_s - \bar{\theta}_4)) \times (\bar{\theta}_s - \bar{\theta}_4) = 0, \quad (9)$$

where C_1, C_2, C_{1T} and C_{2T} are functions of coefficients appearing in (2) to (8). When $\bar{\theta}_s < \bar{\theta}_4$, stable stratification exists, the last two terms drop out, and $\bar{\theta}_s$ is simply given by $\bar{\theta}_s = -C_2/C_1$. When $\bar{\theta}_s > \bar{\theta}_4$, (9) is a quadratic equation. The last two terms deplete energy from the earth's surface. If we first solve (9) without the last two terms, and if the computed $\bar{\theta}_s$ is less than $\bar{\theta}_4$, then this is taken as the solution. However if this gives $\bar{\theta}_s > \bar{\theta}_4$, then the full quadratic equation (9) is solved as such. The true solution must be less than $-(C_2/C_1)$ and greater than $\bar{\theta}_4$. We can also solve (9) by iteration. Both methods give identical results. The first method which is direct and most efficient is used here.

3. The response factor R_F

In experiments, there will be input parameters such as $\bar{r}_s$, $\bar{w}$ etc. (Table 1) and output parameters such as $\bar{H}_S$, $\bar{\theta}_s$, etc. Symbolically we can write for a two-component system

F_C gives rise to R_C,

where F_C is the forcing input for the control experiment and R_C is the response output for the control experiment. The forcing parameters are exogenous (predetermined, external or independent) while the response parameters are endogenous (undetermined, internal or dependent). If we perturb F_C and if the new variables are F_P and R_P respectively, then we can define F_{PF} = Forcing Power Factor = $(F_P - F_C)^2/F_C^2$, and R_{PF} = Response Power Factor = $(R_P - R_C)^2/R_C^2$, when F_C and R_C are non-zero. For large-scale problems we can also define large-scale power factors. In order to study the response characteristics with latitude, we define a forcing latitudinal power factor F_{LPF} as $\langle(F_P - F_C)^2\rangle/\langle\langle F_C^2\rangle\rangle$, and a response latitudinal power factor R_{LPF} as $\langle(R_P - R_C)^2\rangle/\langle\langle R_C^2\rangle\rangle$. F_{LPF} and R_{LPF} can be defined for oceans and land separately. We define an index which we will call the "Response Factor" as:

$$R_F = (R_{LPF}/F_{LPF})^{1/2}.$$

R_F is a measure of the sensitivity of the response to perturbations in various inputs. Alternatively we could utilize the absolute values by taking $F_{PF} = |F_P - F_C|/|F_C|$. However for random perturbations within certain bounds, say $\pm 5\%$, both methods are almost equivalent. Our aim will be to compute R_F, which is the linear response for a unit perturbation of the forcing. With this aim we will describe some experiments.

Two control experiments are performed, one for winter and one for summer, prescribing all the necessary data such as $\bar{T}_D$, $\bar{\theta}_4$, $\bar{\theta}_2$, $\bar{w}$, $\bar{r}_s$, $\bar{c}$ etc. Then we introduce random perturbations of a limited amplitude for each of the parameters in a series of experiments, for winter and summer separately. With the help of these results we determine the linear response factor R_F in each case, and compare them.

4. Experiments for studying R_F and discussion of results

In this section we present the results of the experiments: two control experiments and some perturbation experiments.

4.1. *Experiment (1), control experiment for winter*

We notice that for this problem the input parameters are basically of two types. They are (a) field parameters such as $\bar{\theta}_4$ and (b) empirical constants such as K_0.

In this experiment we basically adopted the empirical constants of Saltzman and Ashe (1976a, b). For the input field parameters $\bar{T}_D$, $\bar{w}$, $\bar{r}_s$, $\bar{c}$, $\bar{\chi}$, and $\bar{r}_a$, the values utilized by Vernekar (1975) and Vernekar and Chang (1978) were adopted. For $\bar{\theta}_4$ and $\bar{\theta}_2$, the observed monthly mean values were utilized (Crutcher and Meserve, 1970). β_R, which is about 0.3, was taken to be a function of latitude. This was done to take into account the variation of the average cloud height with latitude. These values were adopted from Kondratyev (1969). The zonal means of some of the input parameters for this experiment are given in Table 1.

Table 1. *Control experiments. Zonal means of input fields and parameters for January (W) and July (S).* $\bar{\theta}_4 = \bar{\theta}_4(\lambda, \phi)$, $\bar{\theta}_2 = \bar{\theta}_2(\lambda, \phi)$, $\bar{T}_D = \bar{T}_D(\lambda, \phi)$. *The type of surface is indicated with* O *(ocean) or* L *(land)*

Lat.	$\bar{T}_D$	$\bar{\theta}_4$ (W)	$\bar{\theta}_2$ (W)	$\bar{\theta}_4$ (S)	$\bar{\theta}_2$ (S)	$\nu\!\downarrow$	$\bar{r}_a(\bar{c})$ (W)	$\bar{r}_a(\bar{c})$ (S)	β_R	$\bar{r}_s$ (W)	$\bar{r}_s$ (S)	$\bar{w}$ (W)	$\bar{w}$ (S)	$\bar{C}_{TK}$ (W)	$\bar{C}_{TK}$ (S)	SFC
80	266.8	252.3	279.9	268.4	302.0	0.95	0.12	0.83	0.57	0.18	0.10	1.00	1.00	45.00	35.00	O
70	270.4	267.4	285.4	284.3	304.8	1.04	0.37	0.74	0.50	0.18	0.10	1.00	1.00	53.00	46.00	O
60	274.2	273.0	292.1	286.0	306.7	1.15	0.43	0.52	0.41	0.17	0.08	1.00	1.00	59.00	54.00	O
50	277.9	276.4	295.1	288.0	311.8	1.24	0.32	0.53	0.36	0.13	0.07	1.00	1.00	61.00	58.00	O
40	284.5	281.3	300.1	294.5	316.8	1.27	0.32	0.36	0.33	0.10	0.06	1.00	1.00	60.00	56.00	O
30	291.7	289.8	311.5	298.4	320.1	1.29	0.22	0.23	0.32	0.08	0.06	1.00	1.00	56.00	49.00	O
20	296.8	296.9	319.2	300.7	321.0	1.30	0.12	0.27	0.33	0.07	0.06	1.00	1.00	50.00	43.00	O
10	299.3	300.6	321.9	300.0	320.4	1.31	0.10	0.36	0.34	0.06	0.06	1.00	1.00	44.00	35.00	O
0	299.7	301.5	321.7	297.7	320.1	1.34	0.13	0.18	0.35	0.06	0.06	1.00	1.00	36.00	36.00	O
80	260.0	249.1	280.8	267.4	301.9	0.95	0.22	0.81	0.57	0.78	0.62	0.00	0.00	1.40	1.58	L
70	264.0	257.3	285.2	286.3	305.0	1.04	0.22	0.69	0.50	0.72	0.51	0.11	0.15	0.77	1.52	L
60	273.1	260.5	286.7	290.3	309.9	1.15	0.34	0.44	0.41	0.66	0.18	0.17	0.77	0.48	1.54	L
50	278.9	265.7	290.8	296.5	314.0	1.24	0.43	0.40	0.36	0.55	0.18	0.25	0.77	0.43	1.55	L
40	290.1	275.4	299.5	301.5	319.4	1.27	0.33	0.35	0.33	0.30	0.20	0.56	0.70	0.77	1.47	L
30	296.7	287.3	309.4	304.2	323.4	1.29	0.22	0.28	0.32	0.23	0.21	0.61	0.68	0.96	1.44	L
20	300.5	296.2	317.5	303.6	322.1	1.30	0.11	0.29	0.33	0.23	0.19	0.58	0.71	1.00	1.52	L
10	301.7	300.1	320.8	301.8	320.6	1.31	0.09	0.42	0.34	0.22	0.14	0.63	0.91	1.00	1.83	L
0	301.0	301.0	321.4	297.9	320.0	1.34	0.22	0.31	0.35	0.12	0.14	0.95	0.90	1.00	1.80	L

The input fields for this experiment are $\bar{T}_D$, $\bar{\theta}_4$, $\bar{\theta}_2$, $\bar{w}$, $\bar{r}_s$, $\bar{c}$, β_R, $\bar{\chi}$, and $\bar{R}(\phi)$. $\bar{r}_a$ is not an independent input field parameter because it is a function of $\bar{c}$. There are other input parameters such as K_0 which are constants. The output fields are $\bar{H}_{SW}$, $\bar{H}_{LW}$, $\bar{H}_{SM}$, $\bar{H}_{SS}$, $\bar{H}_{SD}$, $\bar{H}_S$, $\bar{H}_L$, $\bar{H}_D$ and $\bar{T}_S$.

We notice the following points which agree with the discussion of Saltzman and Ashe (1976b):

The short-wave radiation energy flux $\bar{H}_{SW}$ (Fig. 1): the short-wave flux field follows latitude circles with a slight perturbation of wavenumber 2 superposed on it due to albedo effects.

The long-wave radiation energy flux $\bar{H}_{LW}$ (Fig. 2): the cold land masses generally gain long-wave radiation energy while the warm oceans lose it. In earlier empirical studies (Budyko, 1974) loss of long-wave energy was generally obtained even over land. In this work the gain is found to be mainly associated with the cloud cover. Hence this result suggests that our empirical parameters β_R or ψ may not be accurate enough.

The mean sensible heat flux $\bar{H}_{SM}$: sensible heat is generally gained by the atmosphere over the oceans. The highest gain is to the east of Greenland. This is due to the combined effect of warm subsurface temperature and relatively low surface albedo, which leads to a strong instability and thus large heat gain by the atmosphere. The other two maxima are to the east of the east coasts of the American and Asian continents.

The synoptic sensible heat flux $\bar{H}_{SS}$: strong centers of sensible heat gain by the atmosphere are found over the east coasts of Asia and Western North America, areas of well-defined storm tracks. This component is found to be far more important than $\bar{H}_{SM}$, especially in middle latitudes. The magnitudes are almost twice those of $\bar{H}_{SM}$ in these regions.

The diurnal sensible heat flux $\bar{H}_{SD}$: strong sensible heat loss by the surface is experienced by equatorial Africa and America, and India where this component is as strong as $\bar{H}_{SS}$.

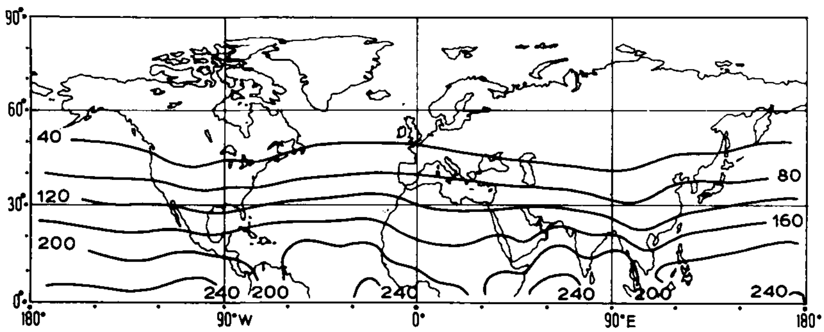

Fig. 1. Short-wave radiation energy flux for January. Contour interval is 40 W m^{-2}.

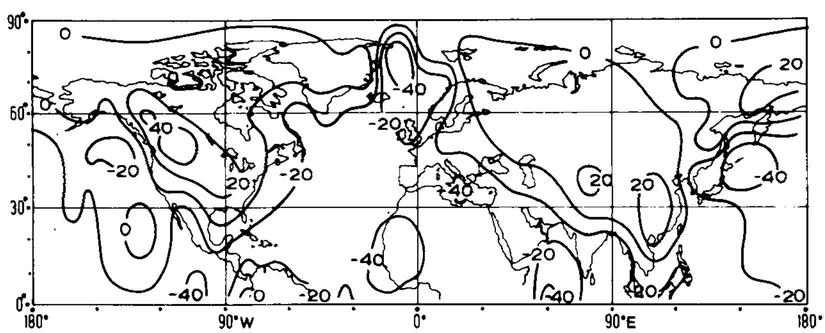

Fig. 2. Long-wave radiation energy flux for January. Contour interval is 20 W m^{-2}.

The total sensible heat flux $H_S = \bar{H}_{SM} + \bar{H}_{SS} + \bar{H}_{SD}$ (Fig. 3): this map shows that there are strong centers to the east of continents and east of Greenland. Comparison with the previous maps shows that in the tropics $\bar{H}_{SD}$ prevails, in the middle latitudes $\bar{H}_{SS}$ is more important, while north of 60° N $\bar{H}_{SM}$ is dominant. Though this map is qualitatively similar to that of Budyko (1974) there are quantitative differences.

Over the east coasts of Greenland and Asia, the computed fluxes are lower by about 25%. Over North America, the maximum flux is not only lower by about 25%, but is also shifted to the west and is situated over the land area. Over the tropics, especially over Africa, the computed flux is twice as strong as that given by Budyko. There can be several reasons for these discrepancies, such as (1) observations can be in error, (2) empirical parameters utilized can be inaccurate, and (3) parameterization may need improvement. Therefore reasons for such discrepancies must be investigated in the future.

The latent heat flux $\bar{H}_L$ (Fig. 4): because of the water availability factor, which is $0 < \bar{w} < 1$ over the land and $\bar{w} = 1$ over the oceans (Vernekar, 1975; Saltzman and Ashe, 1976b), the centers of latent heat gain by the atmosphere occur to the east coasts of the continents and east of Greenland. The equatorial land regions also have strong fluxes because of the diurnal flux and higher water availability. Over the midoceans, $\bar{H}_{SM}$ is the only important part, though it does not reach as high a maximum as $\bar{H}_{SS}$ or $\bar{H}_{SD}$. However because of the vast areas of oceans and because of water availability, most of the latent heat is supplied to the atmosphere by the oceans. The map of $\bar{H}_L$ shows similarity with that of Budyko. However the computed fluxes are weaker as in the case of $\bar{H}_S$.

The subsurface heat flux $\bar{H}_D$ (Fig. 5): the surface, especially over oceans, loses energy in the tropics and gains it in higher latitudes. This might imply meridional ocean currents in the Atlantic and the Pacific Oceans. Over land this flux is negligible.

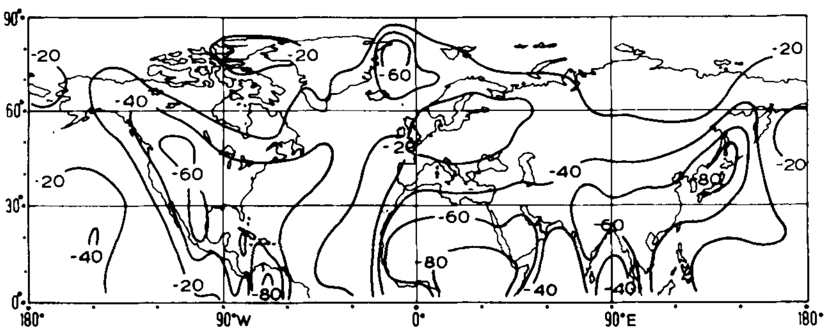

Fig. 3. Total sensible heat flux for January. Contour interval is 20 W m^{-2}.

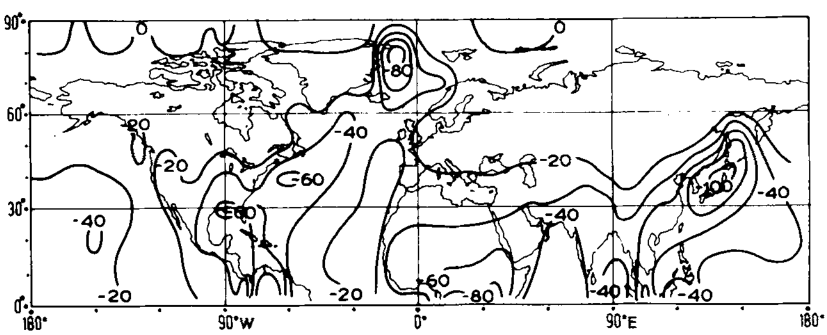

Fig. 4. Latent heat flux for January. Contour interval is 20 W m^{-2}.

The maxima of energy gains in mid-latitudes are comparable to those given by Vernekar (1975) in magnitude and position. However, in the tropics, the energy losses computed here are larger than those given by Vernekar.

The surface temperature $\bar{T}_S$ (Fig. 6): the slightly smoothed $\bar{T}_S$ resembles the observed anemometer level $\bar{T}_S$ maps. The coldest regions are over Western Canada and Eastern Siberia. The computed temperature over Eastern Siberia is −37.5 °C. The observed coldest monthly mean temperature over Eastern Siberia is about −40 °C, according to climatological maps (Vernekar, 1975).

The zonal mean results of this control experiment for land and ocean areas are given in Table 2, from which we infer the following:

1. In general both oceans and land masses lose energy by $\bar{H}_S$ and $\bar{H}_L$.
2. $\bar{H}_D$ plays a dominant role over oceans. This is especially pronounced over the polar regions.
3. Even over land $\bar{H}_D$ is as important as $\bar{H}_S$ and $\bar{H}_L$ over some zones.
4. Over tropical oceans $\bar{H}_D$ is negative to compensate for the incoming solar radiation gain. North of 30 °N $\bar{H}_D$ is positive, compensating the losses by H_{LW}, H_S and H_L. Thus, in higher latitudes the ocean supplies energy to the surface while in the tropics the reverse is true. This implies northward heat transport by oceans at subsurface levels.

4.2. *Experiment (2), control experiment for summer*

This is similar to experiment (1) except that it is for summer conditions. The zonal means are given in Tables 1 (input data) and 3 (results). We note the following points, which again agree with the Saltzman and Ashe (1976b) results:

1. As can be expected $\bar{H}_S$ is less than for winter.
2. In summer too, $\bar{H}_D$ is dominant over oceans.

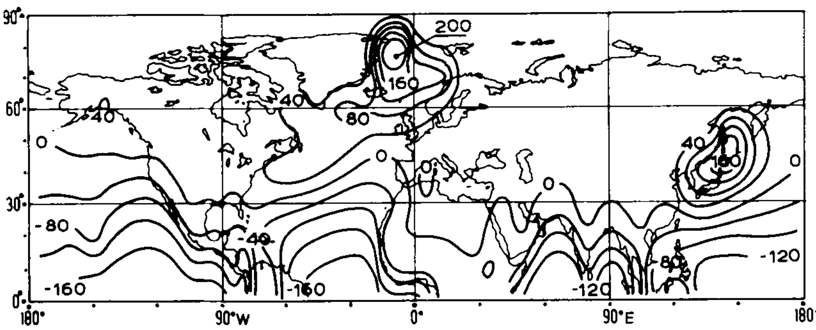

Fig. 5. Sub-surface heat flux for January. Contour interval is 40 W m^{-2}.

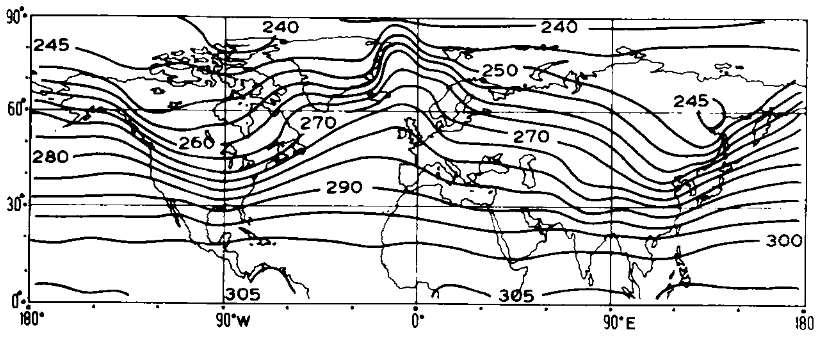

Fig. 6. Surface temperature for January. Contour interval is 5 K.

3. All other results are essentially similar to those of the winter experiment.

For this experiment, we present only $\bar{T}_S$, (Fig. 7) and give the following comments on the results:

The short-wave flux $\bar{H}_{SW}$: the solar radiation flux generally decreases with latitude. Compared to winter, the centers of maximum $\bar{H}_{SW}$ are shifted to the north. In winter the maximum is over the equator while now the maximum occurs around 30 °N.

The long-wave flux $\bar{H}_{LW}$: unlike in winter, the

Table 2. *Control experiment. Zonal means of surface energy balance model results for January. The type of surface is indicated by* O *(ocean) or* L *(land)*

Lat.	$\bar{\theta}_S$	$\bar{H}_{SW}$	$\bar{H}_{LW}$	$\bar{H}_{SM}$	$\bar{H}_{SS}$	$\bar{H}_{SD}$	$\bar{H}_S$	$\bar{H}_L$	$\bar{H}_D$	SFC
80	263.0	0.0	−101.6	−77.1	−19.9	0.00	−97.0	−119.4	318.0	O
70	270.6	0.8	−66.2	−19.2	−36.0	−0.00	−55.2	−66.3	186.9	O
60	274.1	11.7	−37.7	−12.9	−13.5	−0.00	−26.4	−29.8	82.3	O
50	277.1	41.7	−34.9	−10.6	−14.2	−0.00	−24.8	−27.7	45.7	O
40	283.8	75.8	−31.7	−16.8	−21.9	−0.00	−38.7	−45.4	40.1	O
30	292.7	128.4	−16.5	−18.6	−17.4	−0.01	−36.0	−42.0	−33.8	O
20	300.1	189.3	−24.1	−20.6	−8.8	−0.02	−29.5	−33.7	−102.0	O
10	304.2	229.6	−28.6	−21.8	−1.6	−0.03	−23.5	−26.0	−151.5	O
0	305.4	244.3	−19.4	−23.4	−0.4	−0.03	−23.8	−26.0	−174.7	O
80	243.4	0.0	6.7	−2.7	−13.0	0.00	−15.2	0.0	8.7	L
70	249.1	0.3	11.2	−1.2	−16.9	−0.00	−18.0	−1.8	8.2	L
60	255.2	5.6	10.0	−3.5	−16.7	−0.08	−20.4	−3.9	8.6	L
50	264.1	17.7	11.8	−7.6	−21.2	−0.71	−29.5	−7.3	7.3	L
40	275.4	58.5	4.7	−9.8	−26.7	−7.17	−43.6	−26.1	6.5	L
30	287.9	108.0	−7.6	−9.8	−25.3	−24.81	−59.9	−44.4	3.9	L
20	298.7	157.7	−28.8	−16.3	−8.5	−51.10	−76.0	−53.5	0.6	L
10	303.4	194.1	−33.8	−20.8	−1.3	−68.12	−90.2	−69.3	−0.8	L
0	308.0	203.1	−10.3	−44.5	−0.5	−42.19	−87.2	−101.2	−4.4	L

Table 3. *Control experiment. Zonal means of surface energy balance model results for July. The type of surface is indicated by* O *(ocean) or* L *(land)*

Lat.	$\bar{\theta}_S$	$\bar{H}_{SW}$	$\bar{H}_{LW}$	$\bar{H}_{SM}$	$\bar{H}_{SS}$	$\bar{H}_{SD}$	$\bar{H}_S$	$\bar{H}_L$	$\bar{H}_D$	SFC
80	266.3	14.6	56.3	−6.8	−26.1	0.00	−32.9	−38.0	0.0	O
70	272.3	54.5	63.3	1.0	−28.9	0.00	−27.8	−31.6	58.4	O
60	279.1	135.4	35.2	−1.7	−5.5	−0.01	−7.1	−5.3	−158.2	O
50	283.8	145.7	58.8	3.4	−4.4	−0.01	−7.7	−6.0	−190.7	O
40	291.7	214.4	35.4	−5.6	−6.4	−0.02	−12.0	−11.5	−226.3	O
30	299.3	266.4	3.1	−12.3	−2.9	−0.03	−15.2	−15.5	−238.8	O
20	303.4	248.0	0.9	18.4	−0.8	−0.03	−19.3	−20.7	−208.7	O
10	304.4	203.6	11.4	−26.4	−1.2	−0.02	−27.6	−31.3	−158.1	O
0	303.7	228.9	7.6	38.2	−5.3	−0.03	−43.5	−51.5	−126.1	O
80	269.0	6.9	45.4	−12.8	−35.0	−0.03	−47.9	0.0	−4.5	L
70	283.5	36.2	13.1	−4.9	−28.0	−0.99	−33.9	−6.1	−9.3	L
60	295.3	141.2	−32.1	−30.5	−5.3	−15.55	−51.4	−47.0	−10.7	L
50	301.5	165.9	−26.9	−32.3	−8.1	−25.81	−66.2	−61.8	−11.0	L
40	307.4	186.9	−23.6	−37.3	−4.9	−41.88	−84.1	−71.0	−8.1	L
30	309.8	206.3	18.9	−36.5	−2.3	−62.24	−101.1	−80.2	−6.1	L
20	309.0	202.1	−16.4	−35.6	−0.7	−63.16	−99.5	−81.8	−4.2	L
10	308.8	169.5	1.5	−45.0	−4.3	−30.20	−79.6	−87.3	−4.2	L
0	305.2	174.8	11.5	−47.4	−6.3	−33.82	−87.5	−96.3	−2.5	L

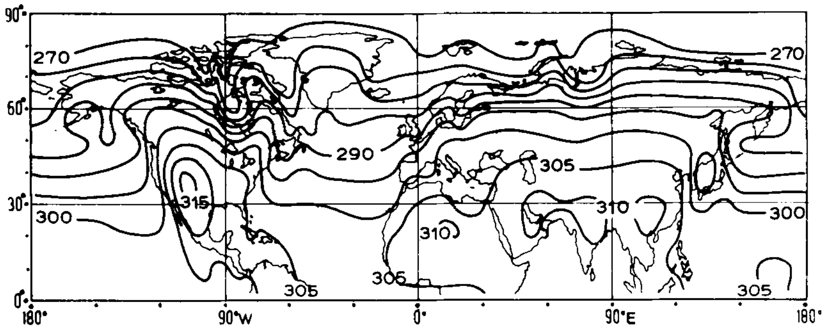

Fig. 7. Surface temperature for July. Contour interval is 5 K.

main centers of energy loss are over the middle of North America and the Mediterranian region. Over some parts of the oceanic areas energy gain takes place.

The mean sensible heat flux $\bar{H}_{SM}$: maximum energy gain for the atmosphere occurs over the Tibetan plateau. Over the West African Coast, the South Eastern Coast of U.S.A., Alaska and Northern parts of South America, weaker centers are found.

The synoptic sensible heat flux $\bar{H}_{SS}$: energy input into the atmosphere by this component occurs mainly North of 60 °N. The maximum occurs around 80 °N over Arctic regions. As can be expected $\bar{H}_{SS}$ is entirely different from winter values.

The diurnal sensible heat flux $\bar{H}_{SD}$: very strong energy input into the atmosphere occurs over the Sahara and the adjoining regions. Another weaker center is situated over the Western part of U.S.A.

The total sensible heat flux $\bar{H}_S$: in general the atmosphere gains heat over the continents. $\bar{H}_S$ is determined mainly by $\bar{H}_{SD}$. This is in accord with the observations of Budyko (1974). Over the Death Valley region, California, and the North West of India, two maxima appear. Over both these regions, the magnitude of the flux maxima is close to that given by Budyko. Because sensible heat flux over these regions is dominated by diurnal flux during this season, the results show that the parameterization of diurnal flux is very satisfactory.

The latent heat flux $\bar{H}_L$: this map is similar to $\bar{H}_S$, except over North Africa because of the water availability factor.

The subsurface heat flux $\bar{H}_D$: all over the Northern Hemisphere, the surface loses heat over the Oceans. This might drive ocean currents of inter-hemispheric nature.

The surface temperature $\bar{T}_S$: highest temperatures occur over the Death Valley desert, the Sahara and India, the Death Valley being the warmest at about 45 °C. Climatological maps indicate that the highest temperatures occur over the Sahara and are about 40 °C. Over the Death Valley region, these maps show temperatures of about 35 °C only. Such differences between the observed and computed maps need to be investigated more in detail. Gradients near the coasts are too steep. The reason might be that land sea breezes are not included in the parameterization.

On the whole we get the impression that the winter climate is to a great extent maintained by $\bar{H}_{SS}$, while the summer climate is maintained by $\bar{H}_{SD}$. The results of the control experiments 1 and 2 for northern hemispheric winter and summer seem to agree to a great extent with observations.

4.3. *Perturbation experiments*

The inputs of the control experiments were perturbed for sensitivity studies. The natural dynamic feedbacks have to be considered for accurate sensitivity studies. However, for such feedback considerations one will have to use regular general circulation models. Here the aim is to arrive at the comparative importance of some parameters in an approximate manner. In this work we decided to introduce the perturbation over all the (λ, ϕ) domain in a random manner within certain bounds, i.e. $\pm 5\%$ of the hemispheric r.m.s. value. We note at the outset that the sensitivity results are model specific, and weakly control experiment dependent.

We perturbed $\bar{T}_D$, $\bar{\theta}_4$, $\bar{\theta}_2$, $\bar{Z}_F$, $\bar{K}_0$, $\bar{\varepsilon}_T$, $\bar{w}$, $\bar{r}_S$, and $\bar{c}$, in a series of experiments, both for winter and summer. The detailed results of a typical experiment due to $\bar{\theta}_4$ perturbation for winter are given in Table 4. We note that the response factor R_F is

Table 4. *Zonal mean values of the response factor R_F for the surface energy balance model results with perturbation in $\bar{\theta}_4$, winter case. The type of surface is indicated by* O *(ocean) or* L *(land)*

Lat.	F	$F_P \times 10^2$	Response factor R_F for									
			$\bar{\theta}_S$	$\bar{H}_{SW}$	$\bar{H}_{LW}$	$\bar{H}_{SM}$	$\bar{H}_{SS}$	$\bar{H}_{SD}$	$\bar{H}_S$	$\bar{H}_L$	$\bar{H}_D$	SFC
80	θ_4	1.16	0.22	0.0	7.9	98.0	98.5	0.0	27.5	31.2	15.4	O
70	$\bar{\theta}_4$	0.65	0.39	0.0	14.5	56.0	116.8	0.0	53.9	55.4	28.7	O
60	$\bar{\theta}_4$	1.00	0.34	0.0	12.4	38.1	81.1	0.0	45.6	47.6	24.5	O
50	$\bar{\theta}_4$	1.02	0.24	0.0	8.8	35.7	58.8	0.0	33.7	34.1	17.8	O
40	$\bar{\theta}_4$	1.01	0.27	0.0	9.8	50.5	50.7	0.0	35.9	37.1	19.2	O
30	$\bar{\theta}_4$	1.01	0.29	0.0	10.8	50.6	59.2	0.0	39.2	40.8	21.0	O
20	$\bar{\theta}_4$	0.93	0.29	0.0	10.8	47.5	49.2	0.0	39.5	40.9	21.1	O
10	$\bar{\theta}_4$	1.00	0.25	0.0	9.2	50.9	18.9	0.0	32.3	34.6	17.6	O
0	$\bar{\theta}_4$	0.94	0.30	0.0	10.9	52.7	43.3	0.0	40.1	40.6	21.1	O
80	$\bar{\theta}_4$	1.17	3.00	0.0	165.9	39.4	215.6	0.0	95.6	0.0	51.1	L
70	$\bar{\theta}_4$	1.06	1.20	0.0	66.5	22.3	74.9	0.0	32.8	8.5	20.0	L
60	$\bar{\theta}_4$	1.05	0.95	0.0	52.4	20.5	58.5	0.0	25.8	6.9	16.1	L
50	$\bar{\theta}_4$	1.08	0.76	0.0	41.8	35.0	38.6	0.0	17.5	9.9	12.7	L
40	$\bar{\theta}_4$	1.02	1.12	0.0	61.6	43.3	56.5	0.0	20.6	20.8	18.6	L
30	$\bar{\theta}_4$	1.05	1.02	0.0	56.1	43.9	50.2	0.0	17.4	19.7	16.1	L
20	$\bar{\theta}_4$	1.10	0.72	0.0	39.8	31.2	22.1	0.0	12.3	13.7	11.3	L
10	$\bar{\theta}_4$	0.98	0.70	0.0	38.4	38.4	14.7	0.0	11.9	13.1	10.7	L
0	$\bar{\theta}_4$	1.15	0.61	0.0	33.7	69.6	32.6	0.0	8.7	14.5	12.8	L

generally a function not only of latitude and type of surface, but also of the output parameter considered. In this table, R_F for $\bar{H}_{SD}$ and $\bar{H}_{SW}$ is zero because they are independent of $\bar{\theta}_4$ in the model. We also note that because of the convergence of the meridians towards the pole and because of weak temperature gradients, the $\bar{H}_{SS}$ response, which depends on temperature gradients, can be unreliable. For instance, over the poles the R_F values for this parameter are sometimes very large. Because $\bar{H}_S$ contains $\bar{H}_{SS}$ as one of the components, the R_F values of $\bar{H}_S$ near the poles can also be large and unreliable. We confine our attention to a region between 10° N to 60 °N. Of all the parameters we chose $\bar{H}_S$, the total sensible heat flux, as an indicator of response. In reality we must consider all output parameters as response indicators. The maximum response factor R_F of $\bar{H}_S$ within this region is considered for intercomparisons.

5. Equivalence of input parameter perturbations

Table 5 gives the maximum R_F of $\bar{H}_S$ between 10 °N and 60 °N both for winter and summer, for each perturbed parameter. The Equivalence Perturbation Percentage (E.P.P.) with respect to $\bar{\theta}_4$, for example, gives us the equivalence of error tolerances in observations of these parameters when we fix the error in any one of them. Thus, suppose we decide to tolerate 0.1% of error in $\bar{\theta}_4$. This is equivalent to 0.15%, 0.35%, 2.3%, 17%, 4.7%, 15%, 2%, and 4.1% errors in $\bar{T}_D$, $\bar{\theta}_2$, $\bar{Z}_F$, $\bar{K}_0$, $\bar{\varepsilon}_T$, $\bar{w}$, $\bar{r}_s$, and $\bar{c}$ respectively.

It is of some interest to note the following:

1. The results are highly sensitive to $\bar{T}_D$ which is generally prescribed. The results suggest that T_D must be given to the same order of accuracy as the atmospheric temperatures, such as $\bar{\theta}_4$.
2. $\bar{Z}_F$ and $\bar{r}_s$ have to be observed, prescribed or predicted with greater accuracy than $\bar{\varepsilon}_T$ or $\bar{c}$.
3. $\bar{K}_0$ and $\bar{w}$ can be prescribed, observed or predicted with ten times less accuracy than $\bar{Z}_F$ or $\bar{r}_s$.
4. $\bar{r}_s$, $\bar{Z}_F$, $\bar{c}$, $\bar{\varepsilon}_T$, $\bar{w}$ and $\bar{K}_0$ are arranged according to their hierarchical order of importance.
5. The tropics, where large energy inputs are involved, are most sensitive.
6. The position of $\bar{\varepsilon}_T$ and Z_F in the hierarchy indicates that the boundary layer must be

Table 5. *Hierarchy of input fields according to model sensitivity evaluated by the response factor R_F. The type of surface* (O = *ocean*, L = *land*) *and the latitude where maximum R_F occurs, are also listed. The equivalent perturbation percentage EPP, relative only to $\bar{\theta}_4$ is given as an example*

Perturbed parameter	R.m.s. value	Max R_F for $\bar{H}_S$						Mean R_F	EPP relative to $\bar{\theta}_4$
		Winter R_F	SFC	Latitude	Summer R_F	SFC	Latitude		
$\bar{\theta}_4$	300 K	40	O	20° N	44	O	20° N	42	1.0
$\bar{T}_D$	300 K	25	O	20° N	29	O	10° N	27	1.5
$\bar{\theta}_2$	300 K	14	L	10° N	10	L	10° N	12	3.5
$\bar{Z}_F$	2000 m	1.5	O, L	40, 30° N	2	L	20° N	1.8	23
K_0	1.0 $m^2 s^{-1}$	0.2	O	20° N	0.3	O	10° N	0.25	170
$\bar{\varepsilon}_T$	1200 $m^3 s^{-1} K^{-1}$	0.9	L	20° N	0.9	L	20° N	0.9	47
$\bar{w}$	0.98	0.4	L	10° N	0.3	L	20, 30° N	0.35	150
$\bar{r}_s$	0.69	2.3	L	10° N	1.4	L	20° N	1.85	20
$\bar{c}$	0.62	0.8	L	10° N	1.3	L	40° N	1.05	41

modelled realistically especially under unstable conditions.

Table 5 shows the results for only one output parameter $\bar{H}_S$. We can have a number of output parameters such as $\bar{H}_D$, $\bar{H}_L$, $\bar{H}_{LW}$ etc. The maximum value of the response factor R_F can be considered as the maximum partial derivative or regression coefficient. If we denote N input parameters by I_i ($i = 1, \ldots, N$), we can write an equation for each of the M output parameters and we get a system as follows:

$$\frac{R_{11}}{R_{11}} I_1 + \frac{R_{11}}{R_{12}} I_2 + \frac{R_{11}}{R_{13}} I_3 \ldots + \frac{R_{11}}{R_{1N}} I_N = \lambda I_1 \approx N I_1,$$

$$\frac{R_{22}}{R_{21}} I_1 + \frac{R_{22}}{R_{22}} I_2 + \frac{R_{22}}{R_{23}} I_3 \ldots + \frac{R_{22}}{R_{2N}} I_N = \lambda I_2 \approx N I_2, \tag{10}$$

$$\cdots\cdots\cdots\cdots\cdots\cdots\cdots\cdots\cdots\cdots$$

$$\frac{R_{MM}}{R_{M1}} I_1 + \frac{R_{MM}}{R_{M2}} I_2 + \frac{R_{MM}}{R_{M3}} I_3 \ldots + \frac{R_{MM}}{R_{MN}} I_N = \lambda I_M \approx N I_M.$$

When $M = N$, eq. (10) is a system of N equations with N unknowns. The weights such as R_{11}/R_{12} etc. are most stable when for small perturbations the perturbation is smallest for the eigenvalue λ. This happens for λ_{max}. Hence the eigenvector of eq. (10) corresponding to the highest eigenvalue $\lambda_{max} \approx N$, gives us the most stable equivalent perturbation vector. When $M > N$, the usual least squares approximation can be utilized.

6. Conclusions

In this study a method of sensitivity analysis to determine a quantitative evaluation of the relative importance of input parameters for forcings on large scales is presented. In particular the results of the experiments described show that in theoretical climate models, for accurate prediction of $\bar{H}_S$, the accuracy of prescription of $\bar{Z}_F$, $\bar{r}_s$, $\bar{c}$, and $\bar{\varepsilon}_T$ has to be higher than that of $\bar{w}$ and $\bar{K}_0$ (Table 5). The surface albedo $\bar{r}_s$ and the height of the friction layer $\bar{Z}_F$, are two input parameters. The results show that these must be determined to the same order of accuracy. In some prediction models $\bar{r}_s$ may be an input parameter but $\bar{Z}_F$ is determined internally. Then it is useful to know how accurately should the model determine $\bar{Z}_F$ for correct weather prediction. In other words the question is how refined and realistic should the model boundary layer package be for good prediction. This question has to be answered keeping in mind the accuracy of the input parameter $\bar{r}_s$, which is externally prescribed. There is probably no advantage in having a very refined boundary layer package, while the input surface albedo is highly inaccurate. Sometimes a refined model may not fare as well as expected (compared to a cruder earlier model) when it is applied to weather prediction. The above reason might explain this to some extent. Physical sophistication of a model cannot be independent of the observational constraints, especially when the model is applied to prediction. The experiments described are very useful in assessing the relative importance of each parameter, i.e. the sensitivity of the model response to the perturbation of a specific input parameter.

Similar experiments can be conducted with GCMs too. These models are being applied for short-range prediction as well as climatic prediction. In such cases there must be compatibility between the accuracy of measurements of various input parameters and the degree of sophistication of the different parts of the GCM.

We used a simple and crude model; a more refined GCM may give a different hierarchy in the input parameters. However simple models can be used as plausible hypothesis producing models, and when appropriately prepared, give easier understanding of specific problems.

7. Acknowledgements

One of the authors, M. Sankar Rao, is grateful to NRC for granting an Associateship at the NASA (GSFC) during which this work was done.

8. Appendix

Notation

A = 273 K;
A_S = horizontal austausch coefficient = 2×10^6 m^2 s^{-1};
A_T = amplitude of the annual surface wave (K);
B_j = amplitude of the jth diurnal harmonic of the incoming solar radiation (W m^{-2}), (j = 1, 2, 3, 4, 5, 6);
BOR = Bowen ratio;
c = cloud coverage;
c_p = specific heat of air at constant pressure = 1.00×10^3 J kg^{-1} K^{-1};
C_{TK} = $\rho_s S K_D^{1/2}$ (J m^{-2} K^{-1} s$^{-1/2}$);
C_5 = empirical constant = 3.8 W m^{-2};
D = any dependent variable;
$\bar{D}$ = $(1/T_A)\int_0^{T_A} D\,dt$ = time average of D;
$\langle D\rangle$ = $(1/2\pi)\int_0^{2\pi} D\,d\lambda$ = zonal average of D;
$\langle\langle D\rangle\rangle$ = $(1/\pi^2)\int_0^{\pi/2}\int_0^{2\pi} D\,d\lambda\,d\phi$ = areal average of D over a hemisphere;
k = R/c_p;
K = eddy coefficient of conductivity for the friction layer (m^2 s^{-1});
K_D = molecular and turbulent thermal diffusivity of the surface material (m^2 s^{-1});
K_0 = K in neutral conditions = 1.0 m^2 s^{-1};
P = annual period = 1 year;
p_l = pressure at level l (l = 1, 2, 3, 4) (mb);
p_s = surface pressure (mb);
P_1 = diurnal period, 1 day;
P_2 = synoptic period, 7 days;
R = gas constant of the atmosphere = 287 J kg^{-1} K^{-1};
$\bar{R}(\phi)$ = mean solar radiation received at the top of the atmosphere (W m^{-2});
r_a = albedo of the atmosphere = $(\alpha_a + \beta_a \bar{c})\bar{c}$;
r_s = albedo of the surface of the earth;
S = specific heat of the surface material (J kg^{-1} K^{-1});
t = time (s);
T_A = averaging time period $\approx$ a month or a season;
T_D = sub-surface temperature at the depth of negligible seasonal variation (K);
T_s = surface temperature of the earth (K);
w = water availability factor ($0 < w < 1$ over the land, $w = 1$ over the oceans);
Z_B = $Z_S + Z_F$, height of the planetary boundary layer (m);
Z_D = depth of the sub-surface layer (m);
Z_F = height of the friction layer (m);
Z_S = height of the lower boundary surface (m);
α = synoptic scale time constant = Newtonian cooling coefficient near the surface level = 2×10^{-6} s^{-1};
α_a = empirical parameter for atmospheric albedo definition, function of latitude;
β_a = empirical constant for atmospheric albedo definition = 0.38;
β_R = parameter expressing cloud effect on long-wave radiation, function of latitude;
γ_c = counter gradient flux parameter (K m^{-1});
ε_T = empirical constant describing the effect of stability on K_0 (= 1200 m^3 s^{-1} K^{-1});

θ_l = potential temperature at level l ($l = 2, 4$) (K);
θ_s = potential temperature at the surface of the earth (K);
λ = longitude;
$\nu\downarrow$ = downward long-wave emissivity of the atmosphere at its mid-level temperature;
ρ = density of air in the friction layer = 1 kg m^{-3};
ρ_S = surface material density (kg m^{-3});
σ = Stefan-Boltzmann constant = 5.67×10^{-3} J m^{-2} K^{-4} s^{-1};
ϕ = latitude;
χ = absorptivity of the atmosphere for short-wave radiation;
ω_1 = diurnal frequency = $2\pi/P_1 = 7.29 \times 10^{-5}$ s^{-1};
ω_2 = synoptic frequency = $2\pi/P_2 = 1.04 \times 10^{-5}$ s^{-1}.

REFERENCES

Budyko, M. I. 1974. *Climate and life.* New York: Academic Press.

Crutcher, H. L. and Meserve, J. M. 1970. Selected level heights, temperatures and dew points for northern hemisphere, Naval Weather Service Command, U.S.A, NAVAIR 50-1C-52.

Kondratyev, K. Y. 1969. *Radiation in the atmosphere.* New York: Academic Press.

Kurihara, Y. 1970. A statistical-dynamical model of the general circulation of the atmosphere. *J. Atm. Sci. 27*, 847–870.

Manabe, S., Smagorinsky, J. and Strickler, R. F. 1965. Simulated climatology of a general circulation model with a hydrologic cycle. *Mon. Wea. Rev. 93*, 769–798.

Saltzman, B. 1968. Surface boundary effects on the general circulation and macroclimate, a review of the theory of quasi-stationary perturbations in the atmosphere. *Meteorol. Monogr. No. 30*, 4–19.

Saltzman, B. and Ashe, S. 1976a. The variance of surface temperature due to diurnal and cyclone-scale forcing. *Tellus 28*, 307–322.

Saltzman, B. and Ashe, S. 1976b. Parameterization of the monthly mean vertical heat transfer at the earth's surface, *Tellus 28*, 323–331.

Saltzman, B. and Vernekar, A. D. 1971. An equilibrium solution for the axially-symmetric component of the earth's macroclimate. *J. Geophys. Res. 76*, 1498–1524.

Vernekar, A. D. 1975. A calculation of normal temperature at the earth's surface. *J. Atmos. Sci. 32*, 2067–2081.

Vernekar, A. D. and Chang, H. D. 1978. A statistical dynamical model for stationary perturbations in the atmosphere. *J. Atmos. Sci. 35*, 433–444.